

Light transport regimes in slow light photonic crystal waveguides

N. Le Thomas, H. Zhang, J. Jágerská, V. Zabelin, and R. Houdré
*Institut de Photonique et d'Electronique Quantique, Ecole Polytechnique Fédérale de Lausanne (EPFL),
 CH-1015 Lausanne, Switzerland*

I. Sagnes and A. Talneau
CNRS/Laboratoire de Photonique et de Nanostructures, Route de Nozay, F-91460 Marcoussis, France
 (Received 1 July 2009; revised manuscript received 26 August 2009; published 28 September 2009)

The dispersive properties of waves are strongly affected by inevitable residual disorder in man-made propagating media, in particular in the slow wave regime. By a direct measurement of the dispersion curve in k space, we show that the nature of the guided modes in real photonic crystal waveguides undergoes an abrupt transition in the vicinity of a band edge. Such a transition that is not highlighted by standard optical transmission measurement, defines the limit where k can be considered as a good quantum number. In the framework of a mean-field theory we propose a qualitative description of this effect and attribute it to the transition from the “dispersive” regime to the diffusive regime. In particular we prove that a scaling law exists between the strength of the disorder and the group velocity. As a result, for group velocities v_g smaller than $c/25$ the diffusive contribution to the light transport is predominant. In this regime the group velocity v_g loses its relevance and the energy transport velocity v_E is the proper light speed to consider.

DOI: [10.1103/PhysRevB.80.125332](https://doi.org/10.1103/PhysRevB.80.125332)

PACS number(s): 42.70.Qs, 72.15.Rn, 42.30.Kq, 42.25.Dd

I. INTRODUCTION

The transport properties of waves, such as electromagnetic waves, matter waves, electronic waves, or acoustic waves, are strongly affected by the disorder present in the propagating medium.^{1,2} The different regimes of wave propagation that can set up due to disorder-induced scattering depend on the relative values of the mean-free path l of the wave, the sample size L and the wavelength λ .

When $l \gg L$ the medium can be considered as homogeneous and the propagating wave undergoes rare scattering events: the corresponding wave transport regime is often ambiguously called the “coherent” regime.^{1,2} In this case, wave equations such as the Schrödinger or the Helmholtz equations offer a straightforward determination of the eigenstates of the wave field, with the wave number k as a good quantum number. This gives access to a well defined dispersion relations $\omega(k)$ between k and the frequency ω . We will prefer here to name this propagating regime the “dispersive” regime. As transport properties are deterministically predicted from the knowledge of such dispersion relations, the dispersive regime is favored for information transmission in modern communication systems.

When $\lambda \ll l \ll L$, the spatial phase of the field is strongly affected by the disordered potential in the medium. After a propagation over several mean-free paths, the multiple-scattering regime takes place. This regime is governed by a diffusion equation for the energy transport of the wave. Investigation of such diffusive or multiple-scattering regime was initiated in astrophysics to understand the electromagnetic wave transport through stellar and interstellar atmospheres.³ In contrast to classical diffusion, the wave diffusive regime is subject to the presence of interference effects with backscattered field contributions as revealed by the enhanced backscattered cone.^{4,5} From the self-consistent theory of localization, these interference effects can be incorporated in a renormalized extensive diffusion constant $D(L, l)$ that depends on the sample size.²

In general, the scattering approach considers only constant index dispersion. However, the dispersive properties of the underlying unperturbed medium can affect a particular wave transport regime.⁶ For instance, anomalous diffusive transmission and reduction of the diffusion constant near the band edge of partially disordered photonic crystals (PhCs) were reported in Refs. 7 and 8, respectively.

In ideal line-defect photonic crystal waveguides, the group velocity $v_g = d\omega/dk$ of guided Bloch modes theoretically vanishes at band edges. This behavior is currently of high interest to develop slow light based devices. Nevertheless, as shown in Refs. 9 and 10, the presence of residual disorder in actual structures strongly affects the group velocity at the band edges. Some of the first experimental investigations of the speed of light transport in line-defect photonic crystal waveguides reported group velocity of $c/50$ and $c/150$,^{11,12} whereas in other types of experiments group velocities lower than $c/1000$ were claimed.^{13,14} Time-of-flight experiments revealed that the lower group velocity was only $c/7$ near band edges in two-dimensional (2D) PhC structures.¹⁵ More recently, some theoretical calculations predicted that group velocities smaller than $c/100$ could not be achieved in so-called W1 or W3 waveguides, (1 and 3 lines defect, respectively), with the current state-of-the-art technology.^{10,16} In addition Engelen *et al.* highlighted two regimes of light propagation featuring a “group-velocity range of $c/7$ down to $c/200$ ” in chirped W1 waveguides.¹⁷

In view of the recent results in the literature, the light transport in slow light structures has to be clarified, prompting a strong need for a convincing experimental signature of the transition between (i) the dispersive regime, where the concept of group velocity applies, and (ii) the diffusive regime. In this paper, we unambiguously identify the dispersive regime and the diffusive regime by probing both the spatial frequency spectra (k space) and the in-line transmission of the waveguide in the vicinity of a band edge. We propose a qualitative description of the experimental data

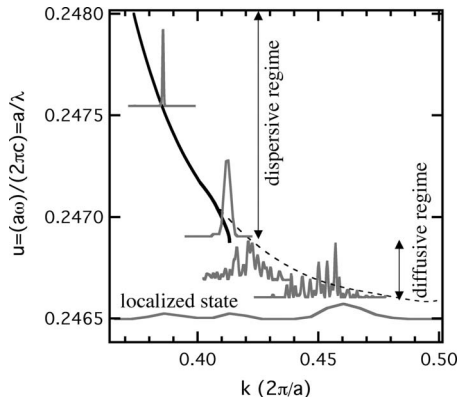


FIG. 1. Definition of the light transport regimes according to their dispersion properties in an actual W1 photonic crystal waveguide (W1 means that one missing line of holes defines the core of the waveguide). Dashed line: dispersion band diagram of the fundamental mode of an ideal W1 waveguide. Black line: schematic representation of the modified dispersion curve due to residual disorder. The corresponding expected angular spectra in the dispersive, diffusive, and localized regimes are superimposed in gray.

based on a standard mean-field theory. We prove that a scaling law exists between the strength of the disorder and the group velocity of the unperturbed medium. As a result, the smallest group velocity achieved among W1 membrane photonic crystal waveguides with different amounts of disorder is around $c/25$. In particular, we highlight the region where the group velocity loses its meaning in favor of the energy transport velocity v_E .

II. QUALITATIVE DISCUSSION OF THE TRANSITION BETWEEN THE DISPERSIVE AND DIFFUSIVE REGIME

In Fig. 1, we show the theoretical dispersion curve of the fundamental guided mode (dashed line) propagating in an ideal W1 photonic crystal waveguide near the boundary of the first Brillouin zone. With this figure, we also give a schematic representation of the expected dispersion curve modified due to an arbitrary residual disorder (dark line) as well as the corresponding spatial frequency spectrum (represented in gray). This plot relies on a mean-field theory and anticipates the effect of the residual disorder on the propagation properties, that we have experimentally measured. In particular, we correlate the dispersive, the diffusive and the strongly spatially localized regimes with the different regions of the modified dispersion curve.

A. Dispersive regime

The dispersive regime, which corresponds to a well defined v_g , is located far enough from the band edge at $k < 0.4 \times 2\pi/a$ where a is the PhC lattice constant. In this regime, the spatial frequency spectrum (angular spectrum) is approximated by a Dirac δ function. When the normalized frequency $u = a/\lambda$ approaches the band edge, the effect of the disorder becomes significant as a result of the slowing down of the light.² It follows that the slope of the dispersion curve

is modified, which sets a lower bound for v_g . Moreover the linewidth of the angular spectrum broadens as a result of the decrease of the mean-free path l , due to the random spatial dephasing of the field. The corresponding shape of the modified dispersion curve can be predicted by analytical perturbative approaches based on mean-field theories and diagram techniques.¹⁸ In this framework, the first moment $\langle \Psi(\omega, k) \rangle$ of the wave field taken over different configurations of the disorder is determined by the Dyson equation. The poles of the corresponding mean Green's function give access to the dispersion curve via the equation $(\omega_0/c)^2 = (\omega(k)/c)^2 + \Sigma(k)$, where ω_0 is the excitation angular frequency. Compared to the unperturbed case, the random dielectric potential leads to an additional term Σ , called the self-energy, which takes into account the correlation induced by disorder in the averaging process of the field. For a homogeneous random medium and in the leading approximation,¹⁹ the self-energy is given by $\Sigma(k) = -i(\omega_0/c)l$. In such media, the dispersion relation is all the more affected that the mean-free path l is small; i.e., that the random fluctuations of the disordered potential are large. In a partially disordered periodic medium as investigated here, $\Sigma(k) \propto \epsilon^2/v_{g0}$ with v_{g0} the group velocity of the unperturbed medium and ϵ the amplitude of the centered Gaussian random function used to model the disordered potential (see the Appendix). The presence of Σ in the equation that determines the dispersion curve sets the lower bound for the group velocity v_g of the perturbed medium. The value of this bound depends on the amount of disorder. The direct relation between $\Sigma(k)$ and v_{g0} reveals that the control parameter to activate different wave transport regimes and to probe their properties can be v_{g0} , much like the concentration or average particle size in powders²⁰ controls the amount of scattering.

B. Diffusive regime

For sufficiently small unperturbed group velocity v_{g0} , the leading approximation does not hold and the dispersion curve cannot be defined. The diffusive regime corresponds to this region where the wave number k cannot be considered as a good quantum number anymore. It results in the formation of specklelike spatial frequency spectra for frequencies close to the band edge ($k > 0.42 \times 2\pi/a$). The disappearance of a dispersion relation between ω and k does not mean that the wave transport vanishes in the diffusive regime in contrast to the strongly spatially localized state regime. In the so-called ladder approximation, the determination of the second moment $\langle \psi(\omega_1, k_1) \psi^*(\omega_2, k_2) \rangle$ of the field from the Bethe-Salpeter equation, shows that the average intensity at a given spatial point is the sum of the Drude-Boltzmann contribution and a contribution known as the “diffuson” contribution.^{19,21} The former contribution, that has an exponential decay and can be neglected after several mean-free path l , corresponds to the dispersive regime.^{2,18} The latter contribution corresponds to the multiple-scattering regime and is associated with the formation of speckles in the spatial frequency spectrum.¹⁹ In this regime, the residual correlations between the specklelike angular spectra over a given angular frequency bandwidth $\Delta\Omega$ allows the definition of an energy transport velocity v_E that can strongly deviate from v_g .^{22,23}

Although the spectral correlations are too weak to generate a clear dispersion curve, the diffusive energy transport can still be efficient in contrast to the strongly spatially localized regime which appears at frequencies ω located below the ideal band edge. Note that waves are always localized in one-dimensional (1D) system subject to a random Gaussian fluctuation provided there are no losses. This means that whatever the energy of the wave, the envelope of the wave function will be localized in space for a sufficiently large length scale of the medium. Here we use the term localization in a more pragmatic way to specify a regime where the envelope of the field is spatially localized in the waveguide with a spatial extension smaller than the length of the waveguide (the spatial extension is defined as the length corresponding to a $1/e$ decrease of the envelope of the field). Such a regime was recently highlighted in Ref. 24.

III. EXPERIMENTAL RESULTS

A. Structures and method

The W1 waveguides experimentally investigated have been fabricated on indium phosphide (InP) semiconductor suspended membrane. A 260-nm-thin InP guiding layer was grown on top of a 1.5 μm InGaAs sacrificial layer, on InP substrate. The W1 photonic crystal waveguides have been patterned in polymethylmethacrylate (PMMA) resist with an ultrahigh-resolution (1.25 nm) Vistec e-beam lithography performed at EPFL. The pattern designed on PMMA was then transferred at CNRS-LPN in an underlying SiO_2 layer used as a mask for N_2/BCl_3 inductive coupled plasma (ICP) process dry etching of the InP membrane layer. After ICP etching and cleaving, the 1.5 μm sacrificial underlying GaInAs layer was selectively etched away to produce the membrane. Supercritical drying in CO_2 was performed to prevent any strain in the structures. The PhC structural parameters were chosen to operate near a wavelength of 1.5 μm . Typical losses reported for W1 waveguides are around 25 dB/cm.²⁵

In order to experimentally determine the dispersion curve and the spatial frequency spectrum of the modes excited in the structure, we have used a high numerical aperture optical Fourier-space imaging technique. This technique, described in details in Ref. 26, provides a direct 2D intensity plot of the angular spectrum of the field emitted from the surface of the sample, as shown in Figs. 2(b)–2(d). As a result, the phase velocities of the modes corresponding to spatial frequencies located inside the bandwidth of the imaging setup are directly and uniquely inferred for a given wavelength. In addition, as the dispersive part of the spatial frequency spectrum of the investigated W1 PhC waveguide is located below the light cone, additional linear probe gratings (LPG) have been implemented along the outer edges of the photonic crystal structure in order to fold the spatial spectrum into the light cone with minimal perturbation as explained in Ref. 27.

The real-space image of the field excited in the W1 PhC waveguide [Fig. 2(a)] shows that the radiated parts mainly come from the center of the waveguide and the probe gratings. The intensity of these contributions is of the same order of magnitude. For this specific image [Fig. 2(a)], the excita-

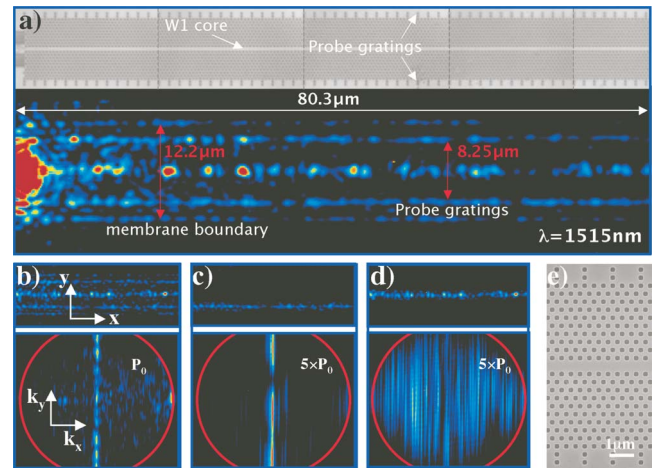


FIG. 2. (Color online) Far-field imaging of the light propagation in a W1 waveguide with identification of the nature of the light transport in k space. (a) Infrared emission pattern radiated from the W1 waveguide (bottom) as well as the optical microscope image at high numerical aperture ($\text{NA}=0.9$) of a typical photonic crystal W1 structure (top). The thin dashed lines mark the optical image stitchings. The large light intensity scattered at the input results from the impedance mismatch at the interface between the access waveguide and the PhC waveguide. (b)–(d) correspond to the real space (top) and Fourier-space (bottom) images of the infrared light radiated from the entire waveguide (b), from only one probe grating, (c) and from only the waveguide center (d), respectively. The excitation power P_0 has been increased fivefold in the Fourier images of (c) and (d). (e) Electron microscopy image of the W1 waveguide ($a=440$ nm) structure. The linear probe gratings (LPGs) consist of a series of two lines of holes periodically spaced with three times the PhC lattice constant [see (a) and (e)]. They are located ten lines apart from the waveguide core to ensure minimal perturbation of the mode whose transverse intensity profile exponentially decreases away from the core.

tion wavelength corresponds to a Bloch mode in the fast light regime (see Fig. 1). This mode is located below the light cone, which implies that no emission from the central part of the waveguide is expected. As shown at the bottom images of Figs. 2(b)–2(d), direct imaging of the angular spectrum corresponding to the emission either from the probe gratings or from the center of the waveguide, enlightens the nature of the scattering processes involved. In particular, it allows us to determine the origin of the scattered light at the center of the waveguide. In Fig. 2(b) the spatial frequency spectrum of all the contributions is measured: it consists of a sharp line and a speckle background that is formed by a random field.²⁸ In Fig. 2(c), an experimental spatial filtering is used to retrieve only the angular spectrum of the field scattered from one of the probe gratings, whereas in Fig. 2(d) only the angular spectrum of the central part is measured. The outcome of this procedure indicates that the sharp line is associated with the field scattered off the probe grating as expected from the folding process of the dispersive part of the field,²⁷ while the central part corresponds only to the speckle part of the spectrum, associated with a random spatial phase of the field.²⁹ Note that the perturbation imposed by the probe grating is less than the intrinsic pertur-

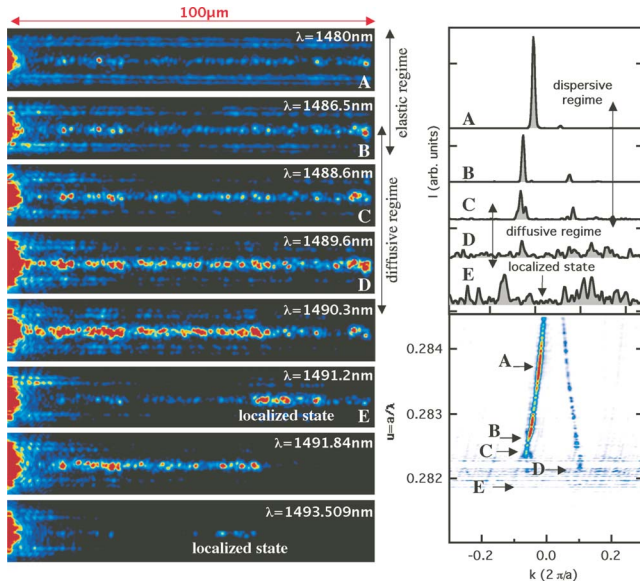


FIG. 3. (Color online) Scanning of the light transport regimes along the dispersion curve. Left: the different light propagation regimes in the W1 photonic crystal waveguide highlighted with the real-space images of the radiated infrared field. Right: the corresponding 2D map representation of the dispersion diagram (at the bottom) as well as some of the angular spectrum profiles (at the top). The 2D representation consists in stacking the angular spectra measured at different frequencies. The position of the intensity maximum (color coded) reproduces the dispersion curve.

bation of the residual disorder, as assessed by the intensity levels of their respective contributions.

B. Frequency scanning of the modes

In Fig. 3, the signatures between the different light propagation regimes are highlighted both with the near-field images and with the far-field spectra. These regimes are progressively activated/deactivated by scanning the frequency ω along the dispersion curve toward the band edge, i.e., by continuously tuning v_{g0} . From the top to the bottom near-field images, we can observe a gradual disappearance of the dispersive contribution at the probe grating in favor of an increasing contribution of the central part.³⁰ The central part emission evolves from an intensity pattern extended along all the waveguide length $L \approx 200 \mu\text{m}$ toward localized intensity patterns identified as localized states. Some of these localized states can be located more than $50 \mu\text{m}$ away from the input of the waveguide with very large Q factors, that we measured to be larger than 10^5 . Such localized states corresponds to states whose wave function is concentrated in a tiny area which can be defined as a dielectric potential trap. The tails of the wave function of these modes have a relatively long penetration length into the dielectric barriers that borders the shallow trap along the waveguide axis, as revealed by the weak out-of-plane losses radiated off the barriers. The spatially localized defect inside the W1 waveguide that localized the mode can be considered similar to the perturbation successfully introduced to create high Q heterostructure PhC cavities.³¹ A second kind of localized states

has been identified as necklace states,^{32,33} for instance at $\lambda=1490.3 \text{ nm}$ and $\lambda=1491.84 \text{ nm}$: their particularity is to exhibit an intensity pattern that begins at the input of the waveguide but abruptly stops at a random position. Their Q factors do not exceed 10^4 . These states can be understood as the onset of the weak localization regime in 1D systems that results from the maximally crossed diagrams in the mean-field perturbation calculation,² while they are responsible for enhanced backscattering in 2D and 3D.

The spatial frequency spectrum observed in the k space, is composed of a main sharp peak in the dispersive fast light regime, as anticipated in the Fig. 1. This peak exhibits a positive first-order dispersion, in line with a forward propagating wave as shown in the 2D map of the angular spectrum. The low intensity symmetric trace comes from the back reflection at the cleaved facet of the output waveguide. When the frequency ω corresponds to the “renormalized” dispersive regime,¹⁸ where the far-field peak broadens, the back-reflection contribution vanishes in favor of speckles contribution.³⁴ Backscattering effects inside the PhC waveguide are not significantly observed in this regime. In the pure diffusive regime, the spatial frequency spectrum exhibits speckles with an approximately constant mean level over the spatial frequency bandwidth. Some residual correlations can still be observed in the 2D map representation for this regime as revealed by several lines that follow the same dispersive trend as the dispersive line of the underlying ideal structure. The transition between the different propagation regimes is not steep and these regimes can coexist inside a given angular frequency bandwidth.

C. Comparison between the transmissions and the dispersion properties

In order to correlate the dispersion properties with the wave transport properties, the dispersion curve $\omega(k)$, the total intensity $I_S(\omega)$ of the emission scattered from the surface along the waveguide as well as the transmitted intensity from the input to the output port of the waveguide $I(\omega)$ are presented in Figs. 4 and 5 for two different waveguides of the same length: the first (Fig. 4) has a large group-velocity cut-off $v_{g \text{ min}} = c/15$ and a large bandwidth $\Delta u = 9 \times 10^{-4}$ for the diffusive regime while for the second, a lower velocity can be assessed $v_{g \text{ min}} = c/25$ and $\Delta u = 6 \times 10^{-4}$ (see Fig. 5). These differences evidence that the unintentional amount of disorder is lower for the second waveguide due to the fabrication process. Note that each case corresponds to only one realization of the disorder of the dielectric map. As a result no comparison of these two structures can be carried out in order to guess some hypothetical specificity of the disorder in one or the other. In both cases, the frequency bandwidths corresponding to the pure dispersive regime and the pure diffusive regime are highlighted in light gray and dark gray shades, respectively. The intermediate gray level region points out the frequency range where the dispersion curves starts to deviate from the theoretical dispersion curve of the underlying ideal structure. The theoretical curve is the outcome of a calculation based on the guided mode expansion model.³⁵

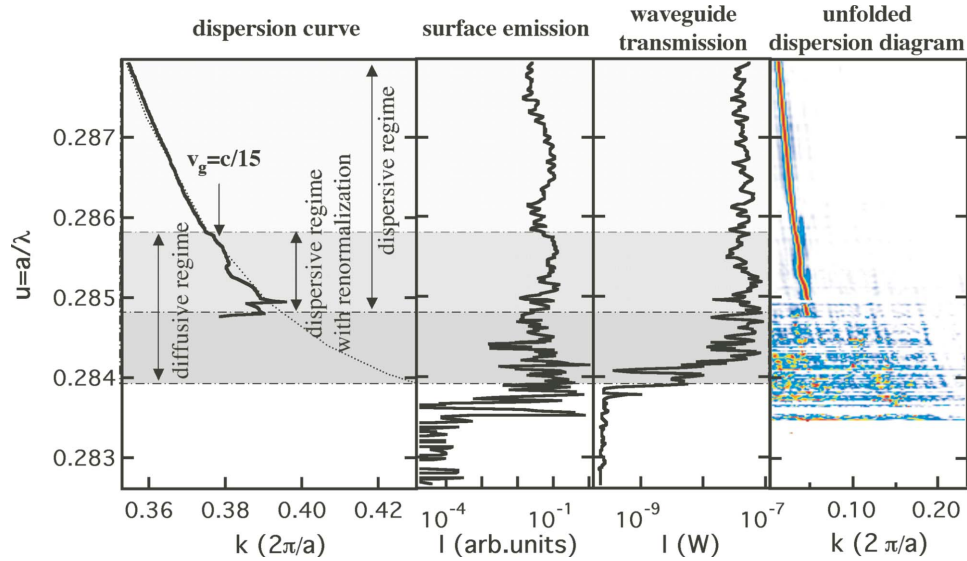


FIG. 4. (Color online) From left to right: experimental dispersion curve (black line), total intensity scattered from the surface of the waveguide at different normalized frequencies u , in-line transmission and the 2D map representation of the unfolded dispersion diagram for a W1 waveguide with lattice constant $a=440$ nm and filling factor $f=0.295$. The dotted line on the left panel corresponds to the theoretical dispersion curve calculated with the guided mode expansion method. The dispersive regime and the diffusive regime are highlighted in light and dark gray, respectively.

To summarize, in the pure dispersive regime the far-field spectrum consists of a sharp peak that follows the variation of the dispersion curve of the ideal structure. In the renormalized regime, the far-field peak broadens, the corresponding dispersion curve differs from the ideal one, with in particular a lower group velocity lower, and a diffusive contribution shows up. In the pure diffusive regime, the peak that allows us to determine the dispersion curve disappears and the far-field spectrum becomes a speckle pattern. As a result, no dispersion curve can be retrieved, whereas the in-line transmission is still efficient. Notes that the difference in the out-of-plane losses between the two waveguides (Figs. 4 and 5) is negligible in the fast light regime, although that the

dispersive properties clearly indicate a difference in the amount of disorder. This implies that the in-plane propagation properties are more sensitive to the residual disorder than the out-of-plane scattering, in line with the recent theoretical results published in Ref. 36.

The direct measurement of the dispersion curve clearly shows that the lower achievable group velocity is limited to around $c/25$ in W1 waveguides subject to typical residual disorder, which agrees with recent investigations based on interferometric techniques.³⁷⁻³⁹ A striking features in the evolution of the dispersive part of the field is its steep extinction. This contrast with the progressive linewidth broadening at the band edge expected when the disordered

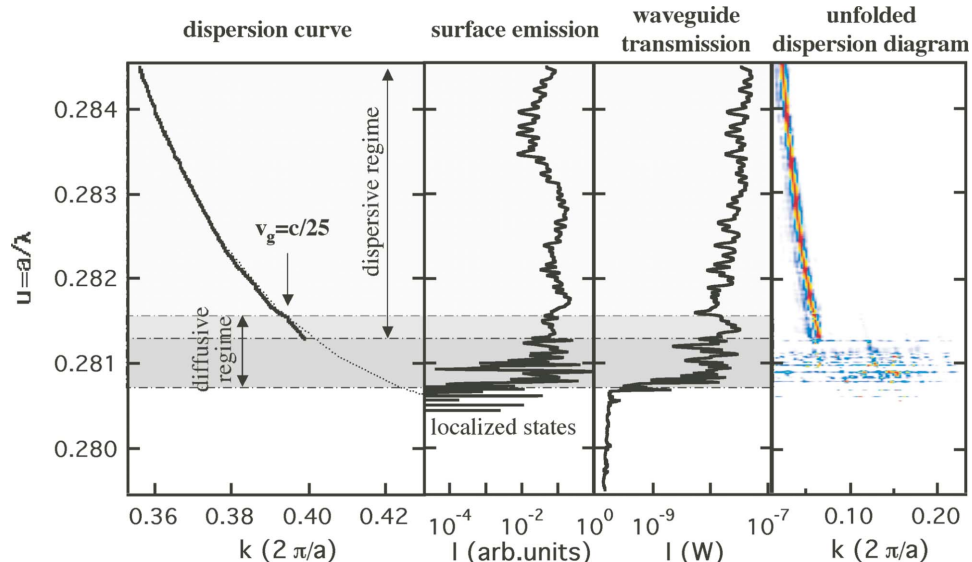


FIG. 5. (Color online) Same as Fig. 4 for a W1 waveguide with a shorter lattice constant $a=420$ nm.

potential and the physical origin of the band edge are uncorrelated.^{40,41} Such an effect for the W1 band edge is directly related with the particular spatial frequency power spectrum $S(k)$ associated with the residual lattice disorder. The $S(k)$ distribution is mainly centered around wave vectors equal to the PhC reciprocal wave vectors.⁴² As a result, when the wave number scales with spatial frequencies located inside the bandwidth of $S(k)$ at half maximum, the coupling of the forward and backward propagating fields located near $k = -\pi/a$ and $k = +\pi/a$, respectively, takes place. Based on this interpretation, the impact of the disorder can be partly overcome with PhC designs where the slow region of the dispersion curve ($v_g \sim c/150$) is located sufficiently far away from the Brillouin-zone boundaries, such as in coupled-cavity waveguides where group indices larger than 150 have been reported.^{43–45}

The second major striking result confirms the consistency of our interpretation: the light transmission through the waveguide is still large in the Pure diffusive regime, especially near the transition where the dispersive part disappears and where no dispersion relation $\omega(k)$ exists anymore. This regime, where the light transport cannot be quantified by the group velocity v_g , is characterized by large fluctuations in the transmitted and scattered intensities.

The perturbative approach is convenient to describe the corresponding intensity transport as the result of multiple-scattering events. It relies however on the eigenstates of the ideal waveguide. In contrast, the present experimental approach allows us to directly measure the spatial frequency spectrum of the actual eigenstates of the disordered dielectric map. These eigenstates exhibit complex wave-vector distributions in k space, especially in the slow light regime. In such a regime, the speed of propagation of a light pulse depends on the correlations between the different k -space spectra inside the angular frequency bandwidth of the incoming pulse. The main correlation effects, that govern the evolution of a wave packet, are included in the two-frequency mutual coherence function $\Gamma(r, \omega, \Omega) = \langle u_{\omega+\Delta\Omega/2}(r) u_{\omega-\Delta\Omega/2}^*(r) \rangle$,⁴⁶ where $u_\omega(r)$ is the complex amplitude of the field. When v_{g0} enters the slow light regime, correlations between the k -space spectra of the eigenstates are strongly affected: the concept of group velocity, where the correlations are maximal, loses its meaning, even before the onset of light localization. Nevertheless, the presence of correlations among the spatial frequency spectra still defines a diffusive regime with a transport velocity v_E . With the data stemming from interferometric methods based on Fabry-Perot oscillations,^{11,12} we speculate that these correlations can still produce a fringe pattern, albeit with a low degree of visibility, like in low coherence interference experiments. In this case, v_g is not expected to be the relevant parameter associated to this fringe pattern, leading possibly to spurious evaluation and overestimated group indices $n_g = c/v_g$. This situation strongly supports the need of a truly experimental determination of the dispersion curve, as presented here, in order to unambiguously settle the lowest achievable group velocity in a given slow light structure and a given technological degree of perfection.

IV. CONCLUSION

In conclusion, the presence of residual disorder generates different light transports near a band edge depending on the value of the group velocity of the underlying ideal structure. In particular, a light transport regime associated with a continuous transmission band is present even when the dispersion curve vanishes. Therefore, a careful distinction between v_g and v_E is required to determine the actual slow-down capability of a specific device for data information management. The direct imaging of the k space in the far field is a reliable approach in order to investigate the lowest group velocity achievable in a photonic structure. Finally, in the same spirit as the investigation of the disorder with matter waves,^{47,48} our approach can be advantageously extended for studying the interplay between disorder and nonlinear interaction, by incorporating for instance quantum wells in the core of the waveguide. Such an approach can also be advantageously extended to 2D systems.⁴⁹

ACKNOWLEDGMENTS

This project was supported by the European network of excellence Epixnet IST (Grant No. 004525), the Swiss NCCR-Quantum Photonics, and the COST action (Grant No. MP0702). We thank Vincenzo Savona for fruitful and enlightening discussions.

APPENDIX: RELATIONSHIP BETWEEN THE SELF-ENERGY AND THE GROUP VELOCITY

In the mean-field calculation of the modal dispersive properties, we assume that the fluctuating part $\mu(\vec{r})$ of the dielectric constant resulting from the disorder is a centered homogeneous random function whose correlation function is expressed as

$$\langle \mu(\vec{r}) \mu(\vec{r}') \rangle = \epsilon^2 \exp(-|r - r'|/\sigma) = \Gamma_\mu(|r - r'|) \quad (\text{A1})$$

with σ the correlation length and Γ_μ the correlation function. Within the tight-binding model, the dispersion curve of the mode is given by

$$(\omega(k)/c)^2 = (\omega_m/c)^2 + 2T \cos(k\Lambda) = (\omega_0/c)^2, \quad (\text{A2})$$

with ω_m the mean frequency of the band, T the transfer integral, and Λ the period of the 1D chain. The Green's function of the unperturbed Helmholtz equation is given by

$$G^{(0)}(r, r'; k_0^2) = \frac{1}{T} \frac{(x - \sqrt{x^2 - 1})^{|l-m|}}{2\sqrt{x^2 - 1}} \quad (\text{A3})$$

as calculated in Ref. 50, with $k_0 = \omega_0/c$ the free space wave number, the normalized energy of the band $x = [k_0^2 - (\omega_m/c)^2]/2T$, $r = l \times \Lambda$ and $r' = m \times \Lambda$, and l and m integers. As a result of the diagrammatic method, the self-energy can be expressed as

$$\Sigma(k) = \epsilon^2 k_0^4 \text{FT}\{G^{(0)}(|r - r'|) \Gamma_\mu(|r - r'|)\}, \quad (\text{A4})$$

where $\text{FT}\{\dots\}$ stands for Fourier transform. With the hypothesis $\sigma \ll \Lambda$, we find

$$\Sigma(k) = \frac{\sigma}{\Lambda} \times \frac{\epsilon^2(\omega_0/c)^4}{T\sqrt{x^2-1}}. \quad (\text{A5})$$

In addition the group velocity can be simply linked to the normalized energy as follows:

$$v_{g0} = \mp i \frac{T\Lambda c}{\sqrt{(\omega_m/c)^2 + 2T \cos(k\Lambda)}} \sqrt{x^2-1}. \quad (\text{A6})$$

With the assumption $2T \ll \omega_m/c$, this last expression can be further simplified as $v_{g0} \approx \mp i \frac{T\Lambda c}{(\omega_m/c)} \sqrt{x^2-1}$, which provides the intended result,

$$\Sigma(k) = \mp \frac{\epsilon^2 c(\omega_0/c)^4 \sigma}{(\omega_m/c) v_{g0}} i \approx \mp \frac{\epsilon^2 c(\omega_m/c)^3 \sigma}{v_{g0}} i. \quad (\text{A7})$$

From this tight-binding approximation, the dispersion effects are included in the self-energy via v_{g0} . By taking the Fourier transform of the Dyson equation, the dispersion relation defined as the poles of the Green's function of the disordered system is given by:

$$x - \cos(k\Lambda) - \frac{1}{2T} \Sigma(k, x) = 0. \quad (\text{A8})$$

This equation points out that the deviation of the dispersion curve from the ideal case is contained in the self-energy whose value diverges near the band edges, i.e., at $x=0$ or $v_{g0}=0$. It also implies that the influence of the residual disorder increases when either the bandwidth $B=4T$ or the group velocity v_{g0} decrease.

-
- ¹A. Ishimaru, *Wave Propagation and Scattering in Random Media* (Academic Press, New York, 1978), Vols. 1 and 2.
- ²P. Sheng, *Introduction to Wave Scattering, Localization, and Mesoscopic Phenomena* (Academic Press, Boston, 1995).
- ³H. C. van de Hulst, *Multiple Light Scattering* (Academic Press, New York, 1980), Vols. 1 and 2.
- ⁴M. P. Van Albada and A. Lagendijk, *Phys. Rev. Lett.* **55**, 2692 (1985).
- ⁵P.-E. Wolf and G. Maret, *Phys. Rev. Lett.* **55**, 2696 (1985).
- ⁶S. John, *Phys. Rev. Lett.* **58**, 2486 (1987); *Phys. Today* **44** (5), 32 (1991); *Comments Condens. Matter Phys.* **14**, 193 (1988).
- ⁷A. F. Koenderink and W. L. Vos, *J. Opt. Soc. Am. B* **22**, 1075 (2005).
- ⁸C. Toninelli, E. Vekris, G. A. Ozin, S. John, and D. S. Wiersma, *Phys. Rev. Lett.* **101**, 123901 (2008).
- ⁹S. Mookherjea and A. Oh, *Opt. Lett.* **32**, 289 (2007).
- ¹⁰N. Le Thomas, V. Zabelin, R. Houdré, M. V. Kotlyar, and T. F. Krauss, *Phys. Rev. B* **78**, 125301 (2008).
- ¹¹M. Notomi, K. Yamada, A. Shinya, J. Takahashi, C. Takahashi, and I. Yokohama, *Phys. Rev. Lett.* **87**, 253902 (2001).
- ¹²Y. A. Vlasov, M. O'Boyle, H. F. Hamann, and S. J. McNab, *Nature (London)* **438**, 65 (2005).
- ¹³H. Gersen, T. J. Karle, R. J. P. Engelen, W. Bogaerts, J. P. Korterik, N. F. van Hulst, T. F. Krauss, and L. Kuipers, *Phys. Rev. Lett.* **94**, 073903 (2005).
- ¹⁴M. Galli, D. Bajoni, M. Patrini, G. Guizzetti, D. Gerace, L. C. Andreani, M. Belotti, and Y. Chen, *Phys. Rev. B* **72**, 125322 (2005).
- ¹⁵C. E. Finlayson, F. Cattaneo, N. M. B. Perney, J. J. Baumberg, M. C. Netti, M. E. Zoorob, M. D. B. Charlton, and G. J. Parker, *Phys. Rev. E* **73**, 016619 (2006).
- ¹⁶B. Wang, S. Mazoyer, J. P. Hugonin, and P. Lalanne, *Phys. Rev. B* **78**, 245108 (2008).
- ¹⁷R. J. P. Engelen, D. Mori, T. Baba, and L. Kuipers, *Phys. Rev. Lett.* **101**, 103901 (2008).
- ¹⁸U. Frish, in *Probabilistic Methods in Applied Mathematics*, edited by A. T. Bharucha-Reid (Academic, New York, 1968), Vol. 1, pp. 75–198.
- ¹⁹B. Shapiro, *Phys. Rev. Lett.* **57**, 2168 (1986).
- ²⁰D. S. Wiersma, P. Bartolini, A. Lagendijk, and R. Righini, *Nature (London)* **390**, 671 (1997).
- ²¹E. Akkermans and G. Montambaux, *Mesoscopic Physics of Electrons and Photons* (Cambridge University Press, Cambridge, UK, 2006).
- ²²M. C. W. van Rossum and T. M. Nieuwenhuizen, *Rev. Mod. Phys.* **71**, 313 (1999).
- ²³B. A. van Tiggelen, A. Lagendijk, M. P. van Albada, and A. Tip, *Phys. Rev. B* **45**, 12233 (1992).
- ²⁴J. Topolancik, B. Ilic, and F. Vollmer, *Phys. Rev. Lett.* **99**, 253901 (2007).
- ²⁵A. Talneau, K. H. Lee, S. Guilet, and I. Sagnes, *Appl. Phys. Lett.* **92**, 061105 (2008).
- ²⁶N. Le Thomas, R. Houdré, M. V. Kotlyar, D. O'Brien, and T. F. Krauss, *J. Opt. Soc. Am. B* **24**, 2964 (2007).
- ²⁷N. Le Thomas, R. Houdré, L. H. Frandsen, J. Fage-Pedersen, A. V. Lavrinenko, and P. I. Borel, *Phys. Rev. B* **76**, 035103 (2007).
- ²⁸J. W. Goodman, *Speckle Phenomena in Optics* (Roberts, Greenwood Village, CO, 2007).
- ²⁹The scattering process that is associated with this spatially inhomogeneous emission occurs mainly at the nonideal row of holes bordering the line defect.
- ³⁰The images in Fig. 3 are typical illustrations of light transport independent of the material used (silicon or indium phosphide waveguide) or technology (e-beam lithography or deep UV lithography), as we know from our several previous experiments.
- ³¹B.-S. Song, S. Noda, and T. Asano, *Science* **300**, 1537 (2003).
- ³²J. Bertolotti, S. Gottardo, D. S. Wiersma, M. Ghulinyan, and L. Pavesi, *Phys. Rev. Lett.* **94**, 113903 (2005).
- ³³P. Sebbah, B. Hu, J. M. Klosner, and A. Z. Genack, *Phys. Rev. Lett.* **96**, 183902 (2006).
- ³⁴In the angular spectrum C, the small line at positive k is not related to the back reflection as confirmed by its slope on the 2D map of the angular spectrum.
- ³⁵L. C. Andreani and D. Gerace, *Phys. Rev. B* **73**, 235114 (2006).
- ³⁶S. Mazoyer, J. P. Hugonin, and P. Lalanne, *Phys. Rev. Lett.* **103**, 063903 (2009).
- ³⁷N. Ozaki, Y. Kitagawa, Y. Takata, N. Ikeda, Y. Watanabe, A. Mizutani, Y. Sugimoto, and K. Asakawa, *Opt. Express* **15**, 7974 (2007).
- ³⁸A. Parini, P. Hamel, A. De Rossi, S. Combríé, N.-V.-Q. Tran, Y.

- Gottesman, R. Gabet, A. Talneau, Y. Jaouën, and G. Vadalà, *J. Lightwave Technol.* **26**, 3794 (2008).
- ³⁹M. Patterson, S. Hughes, S. Combrié, N.-V.-Quynh Tran, A. De Rossi, R. Gabet, and Y. Jaouën, *Phys. Rev. Lett.* **102**, 253903 (2009).
- ⁴⁰V. Savona, *J. Phys.: Condens. Matter* **19**, 295208 (2007).
- ⁴¹R. Zimmermann, E. Runge, and V. Savona, in *Theory of Resonant Secondary Emission: Rayleigh Scattering Versus Luminescence Quantum Coherence, Correlation, and Decoherence in Semiconductor Nanostructures*, edited by T. Takagahara (Academic, New York, 2003), pp. 89–159.
- ⁴²D. Nau, A. Schönhardt, Ch. Bauer, A. Christ, T. Zentgraf, J. Kuhl, M. W. Klein, and H. Giessen, *Phys. Rev. Lett.* **98**, 133902 (2007).
- ⁴³J. Jágerská, N. Le Thomas, V. Zabelin, R. Houdré, W. Bogaerts, P. Dumon, and R. Baets, *Opt. Lett.* **34**, 359 (2009).
- ⁴⁴M. Notomi, E. Kuramochi, and T. Tanabe, *Nat. Photonics* **2**, 741 (2008).
- ⁴⁵D. P. Fussell, S. Hughes, and M. M. Dignam, *Phys. Rev. B* **78**, 144201 (2008).
- ⁴⁶G. Samelsohn and V. Freilikher, *Phys. Rev. E* **65**, 046617 (2002).
- ⁴⁷J. Billy, V. Josse, Z. Zuo, A. Bernard, B. Hambrecht, P. Lugan, D. Clément, L. Sanchez-Palencia, P. Bouyer, and A. Aspect, *Nature (London)* **453**, 891 (2008).
- ⁴⁸R. C. Kuhn, O. Sigwarth, C. Miniatura, D. Delande, and C. A. Müller, *New J. Phys.* **9**, 161 (2007).
- ⁴⁹N. Le Thomas, R. Houdré, D. M. Beggs, and T. F. Krauss, *Phys. Rev. B* **79**, 033305 (2009).
- ⁵⁰E. N. Economou, *Green's Functions in Quantum Physics*, 2nd ed. (Springer-Verlag, Berlin, Heidelberg, New York, 1979).